Eur. Phys. J. Plus (2023) 138:351
https://doi.org/10.1140/epjp/s13360-023-03960-z

THE EUROPEAN PHYSICAL JOURNAL PLUS

Regular Article

Impact of higher-order nonlinear saturation effects on modulation instability in three-core oppositely directed coupler with two negative index material channels

P. Mohanraj[1,a], **R. Sivakumar**[2], **Ancemma Joseph**[3], **Jayaprakash Kaliyamurthy**[1]

[1] Department of Physics, Vel Tech Rangarajan Dr. Sagunthala R and D Institute of Science and Technology, Chennai 600062, India
[2] Department of Physics, Pondicherry University, Puducherry 605014, India
[3] Fatima College, Department of Physics, Madurai, Tamil Nadu 625001, India

Received: 5 November 2022 / Accepted: 7 April 2023

Abstract In this paper, we intend to carry out a detail investigation on influence of higher-order effects on the modulation instability scenario in the three-core triangular (NIM-PIM-NIM) oppositely directed coupler. Upon arriving at the expression for instability gain employing linear stability analysis, particular attention is paid to reveal the impact of stimulated Raman effect and the self-frequency shift over the instability gain and the side band formation in both normal and anomalous instances. The study brings out a novel result that a regime of instability gain still exists in normal group-velocity dispersion even though the modulational frequency (Ω) is zero. However, the benefits in instability at $\Omega = 0$ are zero when the dispersion is anomalous. The self-frequency shift, stimulated Raman effect, and saturable nonlinearity exhibit novel effects of introducing new side lobes and merging the existing side bands paving technique to generate solitary wave/solitons or very brief pulses.

1 Introduction

Nonlinear systems across several physical disciplines exhibit the universal phenomena known as modulation instability (MI), which could readily be perceived as the exponential increase of minor perturbations applied to continuous waves. It is a crucial method for comprehending how the nonlinearity and dispersion of the underlying nonlinear system interact [1–3]. While MI can also be produced for normal dispersion under various physical conditions [4–7], it often occurs in optical fibres for anomalous dispersion [8, 9]. MI frequently has detrimental consequences on optical communication systems [8]. As we look into the application prospects, versatile domains of MI usage can be seen in fibre lasers [10], frequency conversion optimisation [11], ultrashort pulse generation [12], new laser development [13], fibre characterisation [14], supercontinuum generation [15], all-optical switching [16], fibre-optic sensing [17], and so on.

Mode-division-multiplexing (MDM) technology has been developed recently to boost the optical communication system's transmission capacity [18–21]. Correspondingly, there is a renewed curiosity in the examination of the wave transmission in multicore and multimode as the system evolves as the potential new-generation information transmission medium [22–24]. The nonlinearity plays a crucial role in affecting the attributes of MDM system [25–28]. To comprehend the interplay between the nonlinearity and the dispersion of the underlying nonlinear system, rigorous research into MI in multicore and multimode fibres is required. Several studies have already been conducted to investigate MI in few-mode fibres and few-core fibres, particularly in three-core fibre (TCF) [29–35]. For short pulses with width ~ 1 ps or less, among the higher-order nonlinear effects, intrapulse Raman scattering (IRS) and self-frequency shift (SFS) are poignant and proved to be consequential with their optical shock effect and the red frequency shift of soliton [8]. Quite a few studies in metamaterial-fabricated three-core fibres have looked at the influence of IRS and SFS on MI in two-core fibres with the negative refractive core [36–48]. When the input intensity is sufficiently enough in systems such as impurity-added semiconductor fibre and a few polymers, higher-order nonlinear susceptibilities will tend to appear and merge and saturate the nonlinear response. Due to this, the increase in the nonlinearity in such a fibre system is not monotonous, but rather levels off towards saturation at a characteristic power known as a saturation power. Few works have also discovered further useful results while describing the effect of higher-order nonlinear saturation on MI in two-core and three-core fibre systems [49–54]. However, the scenario of three-core fibre with alternating positive/negative refractive indices and the effects of IRS and SS has never been investigated.

The main objective of this paper was a systematic investigation of the impact of SS and IRS on the MI in TCF with traditional saturable nonlinearity. In Sect. 2, we provide the coupled nonlinear Schrödinger equations that govern the propagation of pulses in nonlinear TCF with the SS and IRS effect and talk about the physical significance of the essential parameters. The MI spectrum

[a] e-mail: mohanrajsphysics@gmail.com (corresponding author)

Published online: 23 April 2023

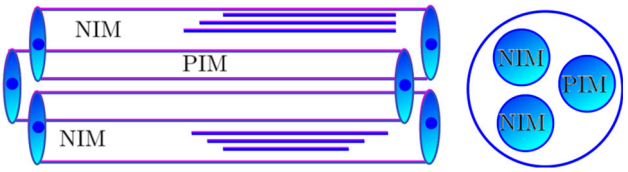

Fig. 1 Schematic representation of three-core triangular coupler with opposite directionality

is then analytically calculated in the presence of SS and IRS using the linear constancy approach, and in Sect. 3, we analyse the implications of SS, nonlinear saturation, and IRS on MI for both anomalous and normal regimes. Finally, in Sect. 5, we provide the crucial findings of the impacts of SS, nonlinear saturation, and IRS on the MI spectrum in TCF.

2 Modal for analytic and classical linear stability technique

2.1 *Modulational instability gain profile* via *coupled nonlinear Schrödinger equations (NLSE)*

We have taken into consideration the schematic replica of the connector invent with three oppositely aligned planes as exposed in Fig. 1 for the sake of our inquiry. It can be conceptualised as a leisurely changing wave packet by means of Ref. [55]. Channels 1 and 3 are conversing in this configuration. References [38, 51, 52] cover other variations. Higher-order nonlinear property becomes noteworthy when the electromagnetic wave propagates within the three cores (NIM-PIM-NIM) with incident intensity sufficiently greater than the verge level. The transmission form has to be tailored appropriately if higher-order nonlinearities such stimulated Raman scattering and self-frequency shift are taken into account [51]. The NLSE described in the following [38, 51, 52] offer the leading theoretical equations for electromagnetic wave transmission in a three-core connector with an opposing directionality.

$$i\varepsilon_1\frac{\partial a_1}{\partial z}+\frac{i}{v_{1g}}\frac{\partial a_1}{\partial t}+\kappa_{12}a_2\exp[i\delta z]+\kappa_{13}a_3+\gamma_1\left(|a_1|^2a_1\right)+iS_1\frac{\partial\left(|a_1|^2a_1\right)}{\partial t}-T_{R1}a_1\frac{\partial\left(|a_1|^2\right)}{\partial t}=0 \tag{1a}$$

$$i\varepsilon_2\frac{\partial a_2}{\partial z}+\frac{i}{v_{2g}}\frac{\partial a_2}{\partial t}+\kappa_{21}a_1\exp[-i\delta z]+\kappa_{23}a_3\exp[-i\delta z]+\gamma_2\left(|a_2|^2a_2\right)+iS_2\frac{\partial\left(|a_2|^2a_2\right)}{\partial t}-T_{R2}a_2\frac{\partial\left(|a_2|^2\right)}{\partial t}=0 \tag{1b}$$

$$i\varepsilon_3\frac{\partial a_3}{\partial z}+\frac{i}{v_{3g}}\frac{\partial a_3}{\partial t}+\kappa_{32}a_2\exp[i\delta z]+\kappa_{31}a_1+\gamma_3\left(|a_3|^2a_3\right)+iS_3\frac{\partial\left(|a_3|^2a_3\right)}{\partial t}-T_{R3}a_3\frac{\partial\left(|a_3|^2\right)}{\partial t}=0 \tag{1c}$$

Channels 1 and 3 are NIM in this instance, but Channel 2 is PIM. The refractive index sign is represented by the characters $\varepsilon_1,\varepsilon_2$, and ε_3. Both $\varepsilon_1=\varepsilon_3=-1$ and $\varepsilon_2=1$ are true in the work. The grouping speeds of connectors 1, 2, and 3 are represented by the variables v_{1g}, v_{2g}, and v_{3g}, respectively. a_1, a_2, and a_3 are used to signify the complex normalised amplitudes. The coefficients of nonlinear coupling strength are κ_{12}, κ_{12}, κ_{13}, κ_{21}, κ_{23}, κ_{32}, and κ_{31}. The letters γ_1, γ_2, and γ_3 stand for the Kerr terms. While T_{R1}, T_{R2}, and T_{R3} stand for the induced frequency shift parameters, S_1, S_2, and S_3 represent the self-steepening parameters.

With a nonlinearity of the Kerr type, the index just varies with respect to the light intensity I, whereas for a nonlinearity of the SNL, the index change is related to the saturation function I/(1 + I). One must take into consideration saturation of the nonlinear refractive index, as in the case of Refs. [38, 56], since saturation recurrently happens even at modest concentration, especially in exceedingly nonlinear resources. The requisite saturation function must first be incorporated into the Maxwell equations before the propagation equation can be obtained. The cubic Kerr factor equivalent of the nonlinear index could alternatively be replaced by the saturating index term. We use a clear-cut method with the relevant adaptation for an oppositely aligned connector in the following because the nonlinear saturation replica for the negative indexed material has previously been dealt with [41, 44, 52].

$$g\left(\Gamma|a_i|^2\right)=\frac{|a_i|^2}{1+\Gamma|a_i|^2} \tag{2}$$

The diffusion factor Γ is connected to the saturation power (P_{sat}) by the equation $\Gamma=1/P_{sat}$ and here $i=1,2,3$.

The saturation and higher-order nonlinear response of the ODSC are accounted for by the modified coupled NLSE, which can be represented as follows:

$$i\varepsilon_1\frac{\partial a_1}{\partial z}+\frac{i}{v_{1g}}\frac{\partial a_1}{\partial t}+\kappa_{12}a_2\exp[i\delta z]+\kappa_{13}a_3+\gamma_1\left(g[\Gamma|a_1|^2]a_1\right)+iS_1\frac{\partial\left(g[\Gamma|a_1|^2]a_1\right)}{\partial t}-T_{R1}a_1\frac{\partial\left(g\left[\Gamma|a_1|^2\right]\right)}{\partial t}=0 \tag{3a}$$

$$i\varepsilon_2\frac{\partial a_2}{\partial z}+\frac{i}{v_{2g}}\frac{\partial a_2}{\partial t}+\kappa_{21}a_1\exp[-i\delta z]+\kappa_{23}a_3\exp[-i\delta z]+\gamma_2\left(g[\Gamma|a_2|^2]a_2\right)+iS_2\frac{\partial\left(g[\Gamma|a_2|^2]a_2\right)}{\partial t}-T_{R2}a_2\frac{\partial\left(g\left[\Gamma|a_2|^2\right]\right)}{\partial t}=0 \tag{3b}$$

$$i\varepsilon_3\frac{\partial a_3}{\partial z}+\frac{i}{v_{3g}}\frac{\partial a_3}{\partial t}+\kappa_{32}a_2\exp[i\delta z]+\kappa_{31}a_1+\gamma_3\left(g[\Gamma|a_3|^2]a_3\right)+iS_3\frac{\partial\left(g[\Gamma|a_3|^2]a_3\right)}{\partial t}-T_{R3}a_3\frac{\partial\left(g\left[\Gamma|a_3|^2\right]\right)}{\partial t}=0 \tag{3c}$$

It is well recognised that obtaining nonlinear spreading curves from the constant wave solutions of the joined equations allows for the convenient disclosure of details on the strength of nonlinearity on the photonic band break [49, 51]. We therefore presume the existence of CW solutions to the basic equations of the structure [51].

$$a_1 = u_1 \mathrm{Exp}\left[i\left(\xi - \frac{\delta}{2}\right)z\right],$$

$$a_2 = u_2 \mathrm{Exp}\left[-i\left(\xi - \frac{\delta}{2}\right)z\right], \tag{4}$$

$$a_3 = u_3 \mathrm{Exp}\left[i\left(\xi - \frac{\delta}{2}\right)z\right].$$

The nonlinear spreading kindred can now be produced by combining Eqs. (1), (2), and (3) with Eq. (4).

$$\mathrm{q} = -\frac{1}{4}u_1^2\gamma_1 + \frac{u_2^2\gamma_2}{2} - \frac{u_3^2\gamma_3}{4} - \frac{u_2\kappa_{12}}{4u_1} - \frac{u_3\kappa_{13}}{4u_1} + \frac{u_1\kappa_{21}}{2u_2} + \frac{u_3\kappa_{23}}{2u_2} - \frac{u_1\kappa_{31}}{4u_3} - \frac{u_2\kappa_{32}}{4u_3}; \tag{5a}$$

$$\delta = -\frac{1}{2}u_1^2\gamma_1 - u_2^2\gamma_2 - \frac{u_3^2\gamma_3}{2} - \frac{u_2\kappa_{12}}{2u_1} - \frac{u_3\kappa_{13}}{2u_1} - \frac{u_1\kappa_{21}}{u_2} - \frac{u_3\kappa_{23}}{u_2} - \frac{u_1\kappa_{31}}{2u_3} - \frac{u_2\kappa_{32}}{2u_3}; \tag{5b}$$

2.2 *Instability gain relation* via *standard linear steadiness method*

The effect of Kerr nonlinearity on MI can be clearly recognised when linear stability analysis is used. A CW must first experience some minor perturbations in order to identify whether it gets weaker or stronger as it spreads. Equation (4) might alter if we have an explanation for the tiny interruptions.

$$a_j = \left(u_j + \alpha_i(z,t)\right)\mathrm{Exp}\left[i\left(\xi - \frac{\delta}{2}\right)z\right] \tag{6}$$

where α_i is a perturbation term ($|\alpha_j| \Delta u_j, i = 1, 2, 3$), and α_i is excessively tiny.

We change Eq. (6) into Eq. (3a, b, and c) and linearism in α_i to make the linear appearance.

$$-i\frac{\partial\alpha_1}{\partial z} + \frac{i}{v_{1g}}\frac{\partial\alpha_1}{\partial t} + \kappa_{12}\alpha_2 - \kappa_{12}f\alpha_1 + \kappa_{13}\alpha_3 - \kappa_{13}\alpha_1 g + L_1\left(\alpha_1 + \alpha_1^*\right) + iu_1^2 S_1\left(2\alpha_1 + \alpha_1^*\right)$$
$$- \mathrm{i}u_1^4 \mathrm{S1}\Gamma\left(3\alpha_1 + 2\alpha_1^*\right) - u_1^2 T_{R1}\left(\alpha_1 + \alpha_1^*\right) + 2u_1^4 T_{R1}\Gamma\left(\alpha_1 + \alpha_1^*\right) = 0 \tag{7}$$

$$i\frac{\partial\alpha_2}{\partial z} + \frac{i}{v_{2g}}\frac{\partial\alpha_2}{\partial t} + \kappa_{21}\alpha_1 - \kappa_{21}\alpha_1 f^{-1} - \kappa_{23}\alpha_2 l^{-1} + \kappa_{23}\alpha_3 + L_2\left(\alpha_2 + \alpha_2^*\right) + iu_2^2 S_2\left(2\alpha_2 + \alpha_2^*\right)$$
$$- \mathrm{i}u_2^4 \mathrm{S2}\Gamma\left(3\alpha_1 + 2\alpha_1^*\right) - u_2^2 T_{R2}\left(\alpha_2 + \alpha_2^*\right) + 2u_2^4 T_{R2}\Gamma\left(\alpha_2 + \alpha_2^*\right) = 0 \tag{8}$$

$$-i\frac{\partial\alpha_3}{\partial z} + \frac{i}{v_{3g}}\frac{\partial\alpha_3}{\partial t} + \kappa_{31}\alpha_1 + \kappa_{32}\alpha_2 - \kappa_{31}\alpha_3 g^{-1} - \kappa_{32}\alpha_3 l + L_3\left(\alpha_3 + \alpha_3^*\right) + iu_3^2 S_3\left(2\alpha_3 + \alpha_3^*\right)$$
$$- \mathrm{i}u_3^4 \mathrm{S3}\Gamma\left(3\alpha_3 + 2\alpha_3^*\right) - u_3^2 T_{R3}\left(\alpha_3 + \alpha_3^*\right) + 2u_3^4 T_{R3}\Gamma\left(\alpha_3 + \alpha_3^*\right) = 0 \tag{9}$$

where $f = \frac{u_2}{u_1}, l = \frac{u_2}{u_3}$, and $g = \frac{u_1}{u_3}$ are the quantities that express how the total power $P = u_1^2 + u_2^2 + u_3^2$ is estranged between the forward and backward transmitting waves. Also, $L_1 = \frac{P}{\left(1+f^2+\frac{f^2}{l^2}\right)}\gamma_1$, $L_2 = \frac{P}{\left(1+\frac{1}{f^2}+\frac{1}{l^2}\right)}\gamma_2, L_3 = \frac{P}{\left(1+l^2+\frac{l^2}{f^2}\right)}\gamma_3, u_1^2 = \frac{P}{\left(1+f^2+\frac{f^2}{l^2}\right)}$, $u_2^2 = \frac{P}{\left(1+\frac{1}{f^2}+\frac{1}{l^2}\right)}$, $u_3^2 = \frac{P}{\left(1+l^2+\frac{l^2}{f^2}\right)}$, $u_1^4 = \frac{P^2}{\left(1+f^2+\frac{f^2}{l^2}\right)^2}$, $u_2^4 = \frac{P^2}{\left(1+\frac{1}{f^2}+\frac{1}{l^2}\right)^2}$, and $u_3^4 = \frac{P^2}{\left(1+l^2+\frac{l^2}{f^2}\right)^2}$.

Look at a typical solution with two side lobe components that can travel both forwards and backwards.

$$\alpha_i[z,t] = C_i \exp[i(kz - \Omega t) + D_i \exp[-i(kz - \Omega t)] \tag{10}$$

where k and Ω are the spatial frequency and modulation frequency, respectively. By totalling Eq. (10) to equations, a set of six linearly associated Eqs. (7–9) that are fulfilled by C_i and D_i is created. The 6×6 determinant of the coefficient matrix must vanish in order for this set to have a nontrivial solution, shown as follows:

$$\begin{pmatrix} M_{11} & M_{12} & M_{13} & M_{14} & M_{15} & M_{16} \\ M_{21} & M_{22} & M_{23} & M_{24} & M_{25} & M_{26} \\ M_{31} & M_{32} & M_{33} & M_{34} & M_{35} & M_{36} \\ M_{41} & M_{42} & M_{43} & M_{44} & M_{45} & M_{46} \\ M_{51} & M_{52} & M_{53} & M_{54} & M_{55} & M_{56} \\ M_{61} & M_{62} & M_{63} & M_{64} & M_{65} & M_{66} \end{pmatrix} \begin{pmatrix} C_1 \\ C_2 \\ C_3 \\ D_1 \\ D_2 \\ D_3 \end{pmatrix} = 0,$$

In this situation, the nonzero matrix coefficients are

$$M_{11} = a^2\mathrm{S1}\Omega + ia^2\mathrm{TR1}\Omega - 2a^4\mathrm{S1}\Gamma\Omega - 2ia^4\mathrm{TR1}\Gamma\Omega + L_1, M_{12} = \kappa_{13}, M_{14} = k + 2a^2\mathrm{S1}\Omega$$
$$+ ia^2\mathrm{TR1}\Omega + \frac{\Omega}{\mathrm{v1g}} - 3a^4\mathrm{S1}\Gamma\Omega - 2ia^4\mathrm{TR1}\Gamma\Omega + L_1 - f\kappa_{12} - g\kappa_{13}, M_{15} = \kappa_{12}, M_{21} = -k - 2a^2\mathrm{S1}\Omega$$
$$- ia^2\mathrm{TR1}\Omega - \frac{\Omega}{\mathrm{v1g}} + 3a^4\mathrm{S1}\Gamma\Omega + 2ia^4\mathrm{TR1}\Gamma\Omega + L_1 - f\kappa_{12} - g\kappa_{13}, M_{22} = \kappa_{12}, M_{24} = -a^2\mathrm{S1}\Omega$$
$$- ia^2\mathrm{TR1}\Omega + 2a^4\mathrm{S1}\Gamma\Omega + 2ia^4\mathrm{TR1}\Gamma\Omega + L_1, M_{26} = \kappa_{13}, M_{32} = b^2\mathrm{S2}\Omega + ib^2\mathrm{TR2}\Omega$$
$$- 2b^4\mathrm{S2}\Gamma\Omega - 2ib^4\mathrm{TR2}\Gamma\Omega + L_2, M_{34} = \kappa_{21}, M_{35} = -k + 2b^2\mathrm{S2}\Omega + ib^2\mathrm{TR2}\Omega + \frac{\Omega}{\mathrm{v2g}} - 3b^4\mathrm{S2}\Gamma\Omega$$
$$- 2ib^4\mathrm{TR2}\Gamma\Omega + L_2 - \frac{\kappa_{21}}{f} - \frac{\kappa_{23}}{l}, M_{36} = \kappa_{23}, M_{41} = \kappa_{21}, M_{42} = k - 2b^2\mathrm{S2}\Omega$$
$$- ib^2\mathrm{TR2}\Omega - \frac{\Omega}{\mathrm{v2g}} + 3b^4\mathrm{S2}\Gamma\Omega + 2ib^4\mathrm{TR2}\Gamma\Omega + L_2 - \frac{\kappa_{21}}{f} - \frac{\kappa_{23}}{l}, M_{43} = \kappa_{23}, M_{45} = -b^2\mathrm{S2}\Omega$$
$$- ib^2\mathrm{TR2}\Omega + 2b^4\mathrm{S2}\Gamma\Omega + 2ib^4\mathrm{TR2}\Gamma\Omega + L_2, M_{51} = \kappa_{31}, M_{53} = c^2\mathrm{S3}\Omega + ic^2\mathrm{TR3}\Omega - 2c^4\mathrm{S3}\Gamma\Omega$$
$$- 2ic^4\mathrm{TR3}\Gamma\Omega + L_3, M_{55} = \kappa_{32}, M_{56} = k + 2c^2\mathrm{S3}\Omega + ic^2\mathrm{TR3}\Omega + \frac{\Omega}{\mathrm{v3g}} - 3c^4\mathrm{S3}\Gamma\Omega - 2ic^4\mathrm{TR3}\Gamma\Omega$$
$$+ L_3 - \frac{\kappa_{31}}{g} - l\kappa_{32}, M_{62} = \kappa_{32}, M_{63} = -k - 2c^2\mathrm{S3}\Omega - ic^2\mathrm{TR3}\Omega - \frac{\Omega}{\mathrm{v3g}} + 3c^4\mathrm{S3}\Gamma\Omega + 2ic^4\mathrm{TR3}\Gamma\Omega$$
$$+ L_3 - \frac{\kappa_{31}}{g} - l\kappa_{32}, M_{64} = \kappa_{31}, M_{66} = -c^2\mathrm{S3}\Omega - ic^2\mathrm{TR3}\Omega + 2c^4\mathrm{S3}\Gamma\Omega + 2ic^4\mathrm{TR3}\Gamma\Omega + L_3$$

whereas dispersion terms are often $v_{1g} \neq v_{2g} \neq v_{3g}$ and coupling coefficients are typically $\kappa_{12} \neq \kappa_{21} \neq \kappa_{23} \neq \kappa_{32} \neq \kappa_{13} \neq \kappa_{31}$, in a manner comparable to [40, 57]. The three-core coupler in this system, however, has alike substantial properties in all three cores aside from the discontinuous refractive indices, where the expressions $\varepsilon_1, \varepsilon_2$, and ε_3 rise in for the index sign. Accordingly, we assume that the cores have the identical pairing strengths of $v_{1g} = v_{2g} = v_{3g} = v_g$. The 6×6 stability matrix's associated determinant vanishes, leading to a polynomial of sixth order.

$$\Omega^6 A + \Omega^5 B + \Omega^4 C + \Omega^3 D + \Omega^2 E + \Omega F + G = 0, \tag{11}$$

The continuous-wave solution's stability is determined by the six roots of Eq. (11). The roots must fall into the negative imaginary fraction domain; this causes the exponential increase in perturbation's amplitude, which is essential for finding MI in one of the sixth-order polynomials roots. The instability gain is produced by the equation:

$$G = |Im(\Omega_{\max})|, \tag{12}$$

where $Im(\Omega_{\max})$ depicts the complex conjugate of $\Omega_{\max}$ and $\Omega_{\max}$ is the polynomial's biggest value's root.

3 Features of the MI spectrum in a three-core coupler channel with opposite directionality

As we get into the details of the three-core coupler with an oppositely orientated MI's dynamics, we start with the instability zone and threshold conditions which are obtained as a function of structure parameters in the forthcoming sections.

3.1 Impact of incident power on the MI

To further explore into the effect of input power on instability gain, Fig. 2 is plotted wherein the instability gain varies as the function of perturbation frequency (Ω) for a few example pump power values in both the anomalous and normal dispersion domains. A substantial steady area between the dual instability regions is produced by a lower pump power. As previously mentioned, a secondary band is emanated from the nonlinear NIM channel, whereas only a primary band at lower Ω levels is emanated from nonlinear PIM channel. The stability area expands as strength and gain increase, and the new side lobes exist in between the two instability regions with respect to less Ω values. Both normal and anomalous dispersion regimes show similar dynamical behaviour, but the generation of the side lobes is different. Thus, the pump power is directly proportional to the MI gain and bandwidth.

3.2 Effect of coupling coefficient on MI

When we look at how the MI gain spectrum is impacted by the coupling terms, we find that the gain is spread throughout a wide range of K with a high-gain zone in the middle at lower values of κ. With increasing coupling terms and MI spectrum, the centre band spreading exhibits an utmost gain shape. As observed in Fig. 3, as the coupling coefficient takes up larger values, it leads to

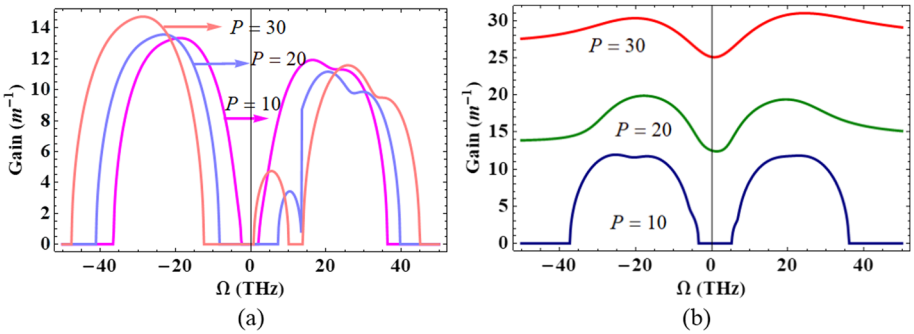

Fig. 2 For various pump power strengths in the **b** normal and **a** anomalous dispersion regimes, the MI gain spectrum is shown

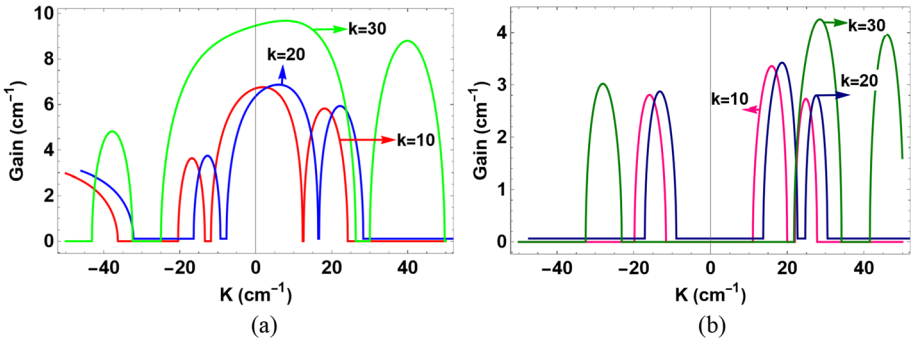

Fig. 3 For various coupling strengths in the **a** normal and **b** anomalous dispersion regimes, the MI gain spectrum is shown

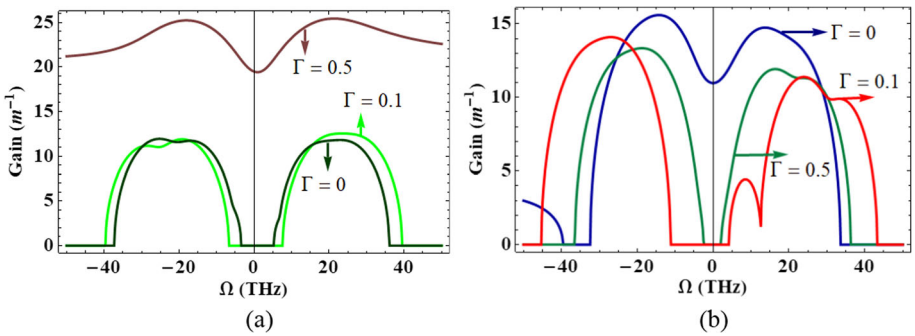

Fig. 4 For various nonlinear saturation strengths in the **a** normal and **b** anomalous spreading domains, the MI gain spectrum is shown

three MI domains with a constant, intermediate domain. The pump power and the union coefficient for instability gain are related in the same way.

3.3 Saturation effects on MI

We provide the MI spectrum for a few typical values in Fig. 4 to emphasise the impact of the nonlinear saturation on the instability spectrum. It is clear that nonlinearity saturation always suppresses the MI by lowering the gain of the instability bands and the bandwidth of the MI.

We provide the MI spectrum for a few example values of Γ in Fig. 4 to illustrate the impact of the nonlinear saturation on the instability spectrum. From the plots, the apparent result that obviously emerges is the saturation of nonlinearity inevitably suppressing the MI by reducing the MI gain and the bandwidth of the instability bands. This is because nonlinearity has been introduced and has become saturated, which has had the effect of decreasing the nonlinear contribution. Therefore, the MI is significantly suppressed in the anomalous dispersion regime alone by a strong saturation. But in the case of the normal dispersion regime, we observed controversy in nature, because the nonlinear saturation can increase the MI strength with the help of increased gain and bandwidth. Thus, the nonlinear saturation effect paves way for a new route of generating soliton or solitary wave in the above-mentioned optical coupler system.

3.4 The effects of self-degeneration on MI

This section discusses the effect of SFS on the MI in an oppositely directed three-core coupler channel. The Raman self-scattering effect is initially omitted by setting ($T_{R1} = T_{R2} = T_{R3} = 0$) and presumptuous that all three NIM-PIM-NIM channels are nonlinear

with γ_1, γ_2, and γ_3. In order to comprehend the effects of SS, we proceed further with the investigations of MI for the various coupler channel configurations shown as follows:

(a) Case: I The SS effect does not influence all channels ($S_1 = S_2 = S_3 = 0$).
(b) Case: II Only the channel PIM is impacted by the SFS effect; the remaining channels (NIM) are unaffected ($S_1 = S_3 = 0; S_2 = 1$).
(c) Case: III The PIM channels are impacted by the SFS effect, but not the NIM ($S_1 = S_3 = 1; S_2 = 0$).
(d) Case: IV The SS effect affects all channels equally and favourably ($S_1 = S_2 = S_3 = 1$).
(e) Case: V The SS effect has an impact on all channels, but in the opposite direction ($S_1 = S_3 = -1; S_2 = 1$).

In both the normal (Fig. 5) and anomalous (Fig. 6) dispersion regimes, we discuss the aforementioned examples.

3.5 Normal dispersion domain ($f > 0$)

Figure 5a plots the volatility growth vs the modulational frequency (Ω) and f lacking the SFS and nonlinear saturation (Γ) effect. Here, we observe that still when the modulational frequency is zero, the gain is still evident for values of $f > 1$. For $f > 1$, there is also a propensity for the four balanced side bands that construct up the growth to detach from one another. Figure 5b shows two symmetric side lobes with respect to $\Omega = 0$. We observed that MI side bands can be reduced by the nonlinear saturation strength. Figure 5c shows the gain spectra for example 2. For a specific choice of modulational frequency (Ω), we can view the compressed MI gain picture in this situation. It is the SFS effect operating exclusively on the PIM channel which brings about the compression of the MI gain there. Further, we introduce the saturable nonlinearity strength like $\Gamma = 0.1$ as shown in Fig. 5d. The dynamical behaviour of MI gain spectrum is enlarged with the help of enlarged MI gain and bandwidth. Additionally, we observed five symmetric side lobes with respect to nil Ω. The SFS result has no impact on the PIM, as shown in Fig. 5e, while in the NIM channels although the frequency of the perturbations is larger, the new instability zones are also visible. The tail of the original MI band contains the new instability bands as well. In the presence of $\Gamma = 0.1$, we observed compressed MI growth spectrum as exposed in Fig. 5f. The strong suppression can help to generate ultrashort pulse and soliton. Each nonlinear channel has an equal sign (case 4). In dissimilarity to example 3 (Fig. 5c), we detected considerable fluctuations in the growth spectrum in Fig. 5g. When all couplers display the SFS effect exclusively having the reverse sign (case 5), Fig. 5i shows the growth spectrum as a function of f and the perturbation frequency. In this case, the MI growth is significantly influenced by the sign of the SFS parameter. Furthermore, we observe that the MI side bands are severely suppressed by the SFS effect amplifying side bands and saturation. SS and nonlinear saturation can produce novel side lobes, alter or merge alive side lobes, and offer a novel method for producing ultra brief pulses or solitons, as our research unambiguously shows.

3.6 Anomalous dispersion scenario ($f < 0$)

We consider the possibility of an anomalous spreading domain ($g < 0$, $l < 0$, and $f < 0$). The main difference between this and regular spreading is that there is no instability increase for the line with perturbation frequency $\Omega = 0$ as observed in Fig. 5. Figure 6a depicts the gain spectrum in instance 1. For all values of f, the MI can be seen in the MI gain's expanded image. As we increase the severity of the nonlinear saturation effect, the two symmetric side lobes transform into four side bands with respect to the perturbation frequency, as shown in Fig. 6b. If the SS effect only affects the channel PIM but not the other NIM channels, as shown in Fig. 6c, we observe that MI dynamical behaviour generates the similar quantity of part bands as those shown in Fig. 5b at the outset. We noticed a widened MI gain profile in the situation of nonlinear saturation. In instance 3, the SFS impact only has an influence on the NIM channels but has no impact on the PIM. Due to the SFS parameter, a larger photograph of MI growth and more side bands are produced with a greater modulational frequency. Therefore, it is obvious that SFS has extended the MI creating area. The same type of MI dynamical behaviour is shown in Fig. 6f with a decreased MI growth profile. Look at Fig. 6g, where the SFS effect applies to all channels equally. We notice substantial differences in the gain range with identical MI kinetics, in contrast to Fig. 5g. In Fig. 6i, all couplers are impacted by the SFS effect, but the indicators are in opposition to one another (case 5). As seen in the normal dispersion regime, the entire working scenario of gain spectrum is essentially similar by raising the amount of instability zones (side bands) and significantly diminishing modulational frequency (case 5). As shown in the anomalous and normal dispersion domains, we can see that the sign of SFS has a crucial role and gain spectra are noticeably sensitive to it.

3.7 Intrapulse Raman scattering's function in MI

The foregoing section leads to the inference that the SFS contribution in a three-core oppositely directed coupler with two negative indexed channels can be very much chosen to control MI and the scrutiny into the result is given in the following. MI may be altered by adjusting the IRS impact also. First, to visualise the scenario in the absence of SFS, the SFS parameters are ignored and gain is plotted as function of the IRS parameter. Figure 7 illustrates the MI gain spectra as a function of the modulation frequency (Ω) and IRS for the anomalous and normal dispersion regimes. It is evident that, in accumulation to the typical invariable MI lobes, the addition of IRS grades in variable lobes on the superior frequency area. Further, we also perceive that in both anomalous and normal scenarios, as the strength of IRS gets increased, the gain of the Raman band also increases. In this case, the MI gain is significantly

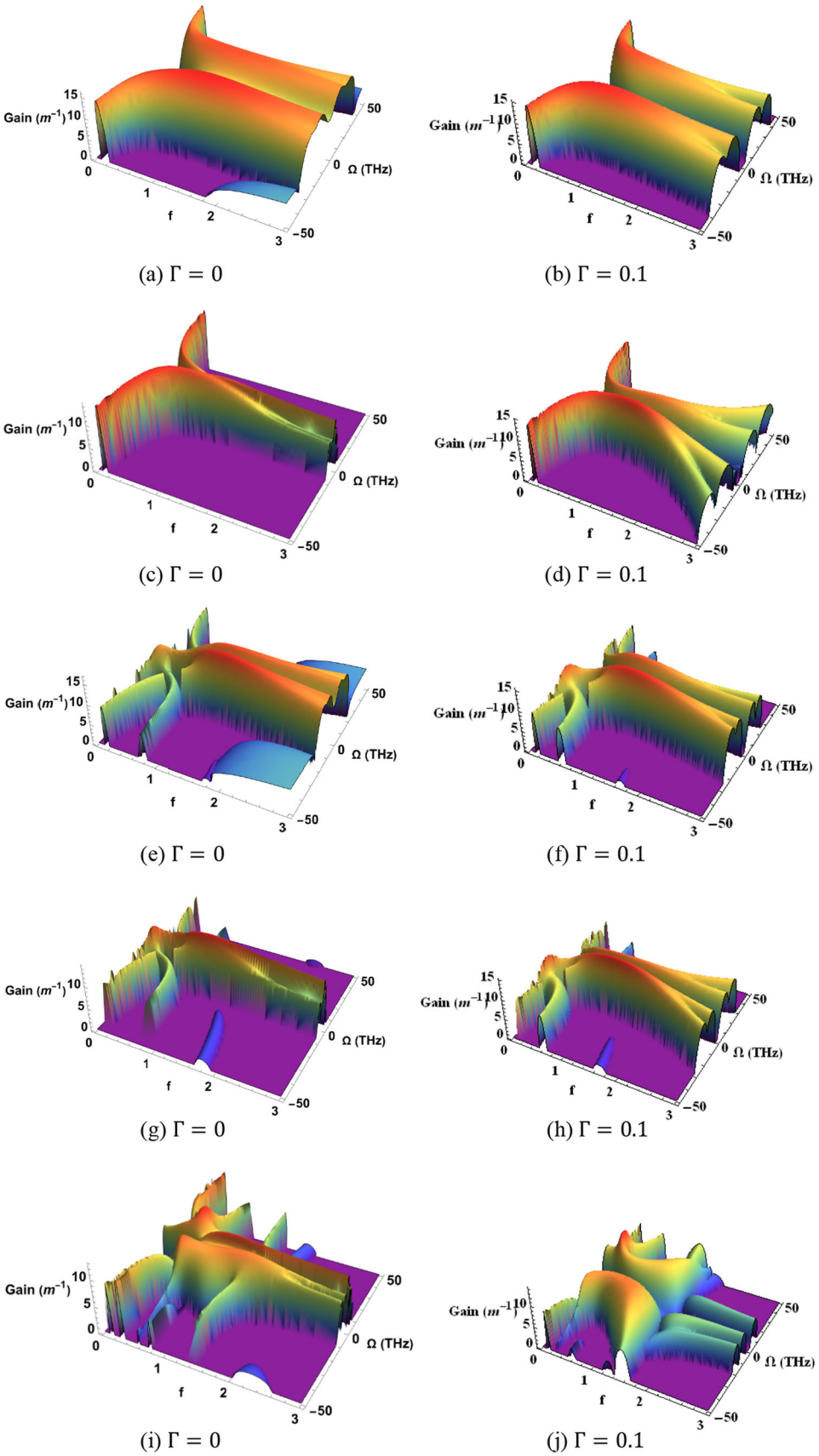

Fig. 5 The stability gain spectra of several SS combinations, such as **a–b** $S_1 = S_2 = S_3 = 0$, **c–d** $S_1 = S_3 = 0$ and $S_2 = 1$, **e–f** $S_1 = S_3 = 1$ and $S_2 = 0$, **g–h** $S_1 = S_2 = S_3 = 1$, and **i–j** $S_1 = S_3 = -1; S_2 = 1$ in the normal dispersion regime ($f > 1$). Other nonlinear parameters are P $= 10$, $\kappa = 10$, $T_{R1} = T_{R2} = T_{R3} = 0$ and $\gamma_1 = \gamma_2 = \gamma_3 = 1$

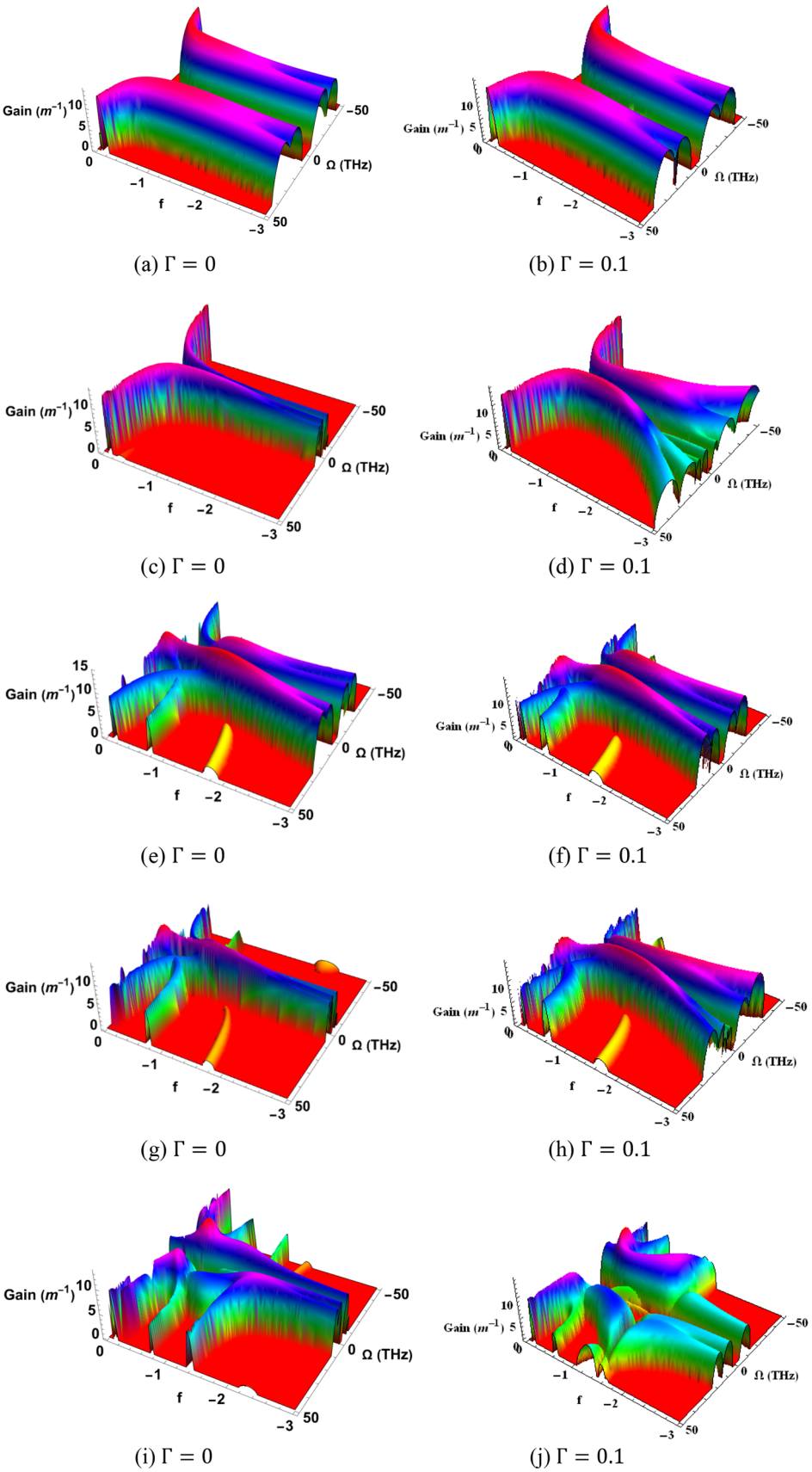

Fig. 6 The stability gain spectra of several SS combinations, such as **a–b** $S_1 = S_2 = S_3 = 0$, **c–d** $S_1 = S_3 = 0$ and $S_2 = 1$, **e–f** $S_1 = S_3 = 1$ and $S_2 = 0$, **g–h** $S_1 = S_2 = S_3 = 1$, and **i–j** $S_1 = S_3 = -1; S_2 = 1$ in the anomalous dispersion regime ($f < 1$). Other nonlinear parameters are $P = 10$, $\kappa = 10$, $T_{R1} = T_{R2} = T_{R3} = 0$, and $\gamma_1 = \gamma_2 = \gamma_3 = 1$

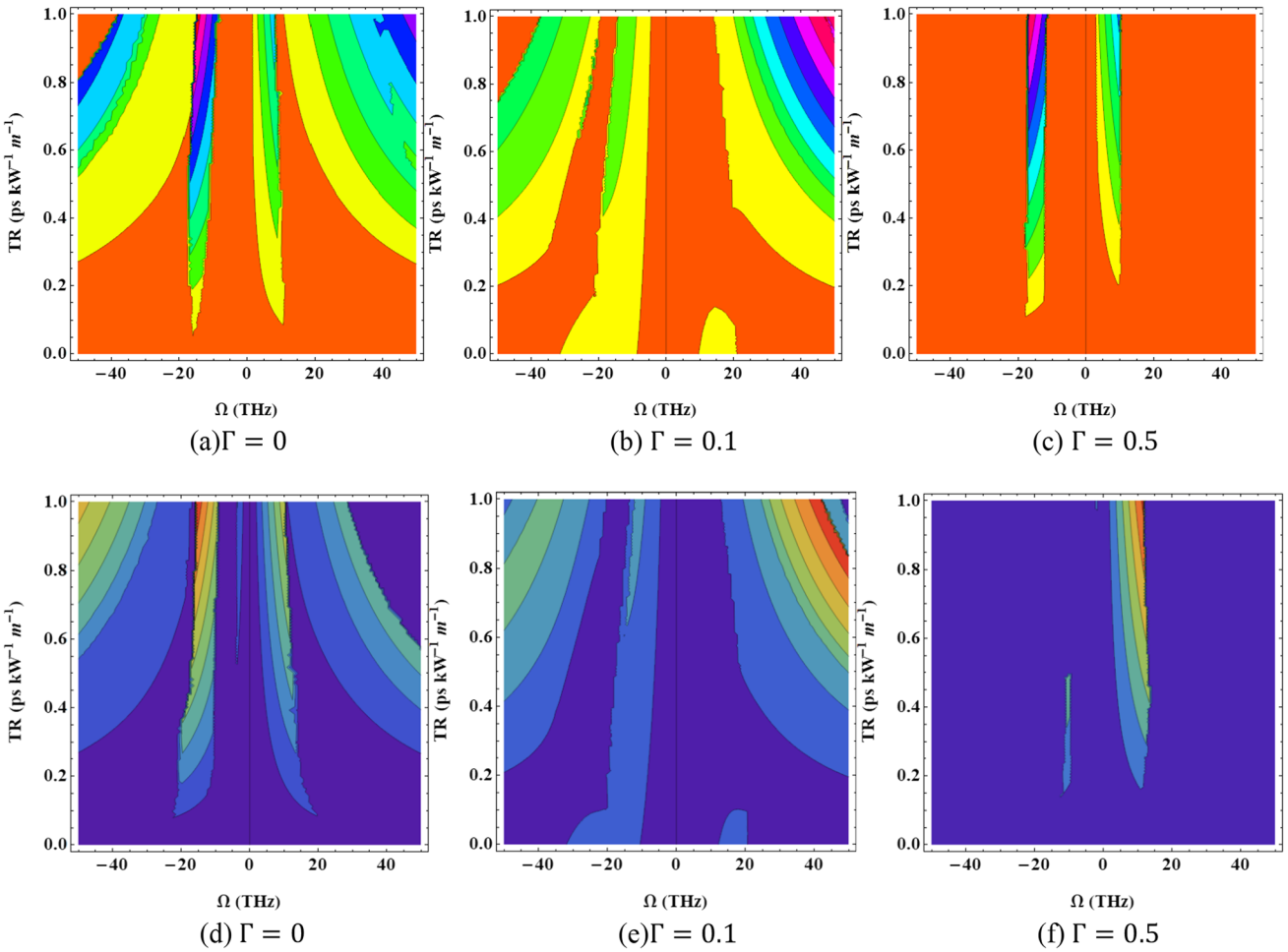

Fig. 7 For different nonlinear saturation strengths, stability growth spectrum illustrates the impact of IRS. **a–c** Normal and **d–f** abnormal spreading domains. The remaining coefficients are $\kappa = 10$, $P = 10$, $S_1 = S_2 = S_3 = 0$, and $\gamma_1 = \gamma_2 = \gamma_3 = 1$

influenced by the potency of the IRS factor. Further, we introduce nonlinear saturation (Γ) into IRS effect, and the two kinds of MI (parametric and Raman) bands disappear with respect to perturbation frequency as shown in Fig. 7b. Interestingly, we add more strength like $\Gamma = 0.5$, and both kinds of bands are completely suppressed. The similar kinds of dynamical behaviour are observed in the abnormal dispersion regime (7d–f). This strong suppression is indeed a novel route for generation of solitons or ultrashort pulses.

3.8 Intrapulse Raman scattering, self-steepening, and their combined effects on MI

In Fig. 8, the united impacts of SS and intrapulse Raman dissemination on MI are examined for both the anomalous and normal spreading regimes in a three-core double-doped connector with a dual NIM connector. As a function of modulational frequency (Ω) and f, Fig. 8 displays the instability growth profile for various saturation strengths, permanent SS, and IRS effect. Figure 8a displays the MI spectrum for IRS potency. The side lobes with the highest MI increase were determined to be one symmetric and non-conventional. The MI gain grew while the kinetic deeds varied as the nonlinear saturation parameter's strength was increased. We observed several MI dynamics in the anomalous case with an expanded MI spectrum (Fig.8d–f). The power of the IRS, SS, and saturation parameters in this case is essential to the MI growth. Additionally, the impacts of the SS, saturable nonlinearity, and IRS result in enhanced side lobes and significantly disturbed frequencies. Our work thus strongly ascertains that SS, nonlinear saturation, and IRS are all capable of generating unique techniques for generating very short pulses or solitons, as well as new side bands, and combinations of side bands.

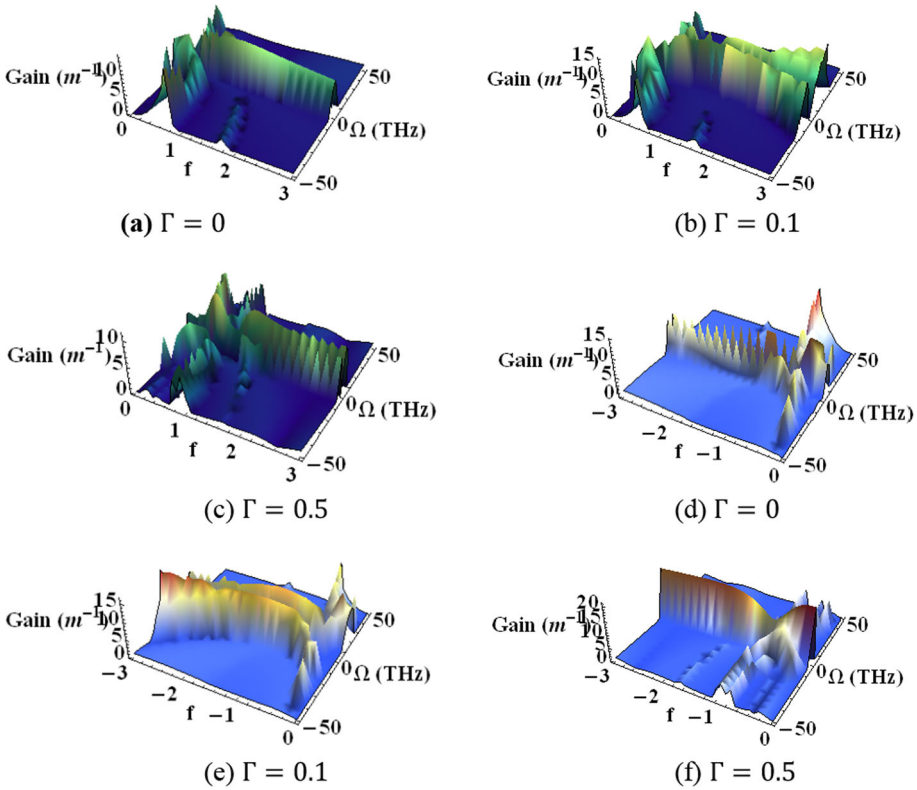

Fig. 8 For different nonlinear saturation strengths in both **a**–**b** normal and **c**–**d** anomalous, the instability growth variation depicts the collective impacts of IRS and SS. Other nonlinear variables include $S_1 = S_2 = S_3 = 1$, $T_{R1} = T_{R2} = T_{R3} = 0.1$, $P = 10$, and $\kappa = 10$

4 Conclusion

In this paper, we have carried out a linear stability analysis to explore the instability scenario in an oppositely directed coupler with higher nonlinear effects. The study of the coupled mode equations encompasses both the anomalous and normal dispersion regimes. While the normal dispersions throw an instability gain scenario even in the absence of perturbation, the instability gain in the case of an abnormal regime is nullified at vanishing modulational frequency. Our investigation into the effects of the self-frequency shift, nonlinear saturation, and stimulated Raman scattering revealed that these processes expand existing instability zones and heighten modulation instability. Because of nonlinear saturation, SS might change or merge existing side bands. We noticed two different types of MI bands, such as the parametric and Raman bands, in the case of IRS. However, the MI side bands can be significantly reduced by nonlinear saturation. However, the saturation effect significantly changes the MI generation in both the anomalous and normal dispersion regimes. Both SS and IRS effects can introduce new side lobes and merge existing side bands. As a result, these occurrences present a novel way to generate solitons or super brief pulses. Furthermore, self-steepening, nonlinear saturation, and intrapulse Raman scattering effects are different for the abnormal and normal dispersion regimes.

Acknowledgements PM expresses gratitude to the UGC for the financial support under the RGNF initiative. One of the authors, RS, would like to recognise DST in part for the FIST money provided by order SR/FST/PSII-021/2009 dated 13 August 2010. Using this money, a straightforward computer cluster facility was constructed. This essay was created with Prof. K. Porsezian's love and support in memory of one of the co-authors who passed away recently.

Data availability The data that has been used is confidential.

Declarations

Conflict of interest The sharing of data is not relevant because no datasets were produced or examined for this subject.

References

1. O. Kimmoun, H.C. Hsu, B. Kibler, A. Chabchoub, Nonconservative higher-order hydrodynamics modulation instability. Phys. Rev. E **96**(2), 022219 (2019)

2. N.A. Chowdhury, M.M. Hasan, A. Mannan, A.A. Mamun, Nucleus-acoustic envelope solitons and their modulational instability in a degenerate quantum plasma system. Vacuum **147**, 31–37 (2018)
3. I. Ferrier-Barbut, M. Wenzel, M. Schmitt, F. Bottcher, T. Pfau, Onset of a modulational instability in trapped dipolar Bose-Einstein condensates. Phys. Rev. A **97**(1), 011604 (2018)
4. X. Zhong, K. Cheng, K.S. Chiang, Modulation instability with arbitrarily high perturbation frequencies in metamaterials with nonlinear dispersion and saturable nonlinearity. J. Opt. Soc. Am. B **31**(7), 1484–1493 (2014)
5. A. Canabarro, B. Santos, B. de Lima Bernardo, Modulation instability in non instantaneous Kerr media with walk-off and cross-phase modulation for mixed group-velocity-dispersion regimes. Phys. Rev. A **93**(2), 023834 (2016)
6. B. Kibler, F. Amrani, P. Morin, A. Kudlinski, Cross-phase-modulation-instability band gap in a birefringence-engineered photonic-crystal fiber. Phys. Rev. A **93**(1), 013857 (2016)
7. M.R.S. Tchio, S. Abdoulkary, A. Mohamadou, Modulation instability induced by high-order dispersion to a coupled nonlinear Schrödinger equation in a single-mode optical fiber with Kerr nonlinearity. Phys. Scr. **94**(3), 035207 (2019)
8. G.P. Agrawal, *Nonlinear Fiber Optics* (Academic Press, Burlington, 2007)
9. A.E. Kraych, P. Suret, S. Randoux, Nonlinear evolution of the locally induced modulational instability in fiber optics. Phys. Rev. Lett. **122**(5), 054101 (2019)
10. G.D. Shao, X. Hu, J. Guo, Y.F. Song, L.M. Zhao, D.Y. Shen, D.Y. Tang, Cavity-assisted modulation instability lasing of a fiber ring laser. Appl. Phys. B-Lasers O. **125**(1), 5 (2019)
11. A. Bendahmane, A. Mussot, A. Kudlinski, P. Szriftgiser, M. Conforti, S. Wabnitz, S. Trillo, Optical frequency conversion in the nonlinear stage of modulation instability. Opt. Express **23**(24), 30861–30871 (2015)
12. D.Y. Tang, J. Guo, Y.F. Song, L. Li, L.M. Zhao, D.Y. Shen, GHz pulse train generation in fiber lasers by cavity induced modulation instability. Opt. fiber Technol. **20**(6), 610–614 (2014)
13. X.M. Liu, Broad and tunable multi wavelength fiber laser at the assistance of modulation-instabilityassisted four-wave mixing. Laser Phys. **20**(4), 842–846 (2010)
14. J. Fatome, S. Pitois, G. Millot, Measurement of nonlinear and chromatic dispersion parameters of optical fibers using modulation instability. Opt. Fiber Technol. **12**(3), 243–250 (2006)
15. C. Lei, A. Jin, R. Song, Z. Chen, J. Hou, Theoretical and experimental research of supercontinuumgeneration in an ytterbium-doped fiber amplifier. Opt. Express **24**(9), 9237–9250 (2016)
16. J.R. Ott, M. Heuck, C. Agger, P.D. Rasmussen, O. Bang, Label-free and selective nonlinear fiber optical bio-sensing. Opt. Express **16**(25), 20834–20847 (2008)
17. M.N. Islam, S.P. Dijaili, J.P. Gordon, Modulation-instability-based fiber interferometer switch near 1.5 μm. Opt. Lett. **13**(6), 518–520 (1988)
18. X. Han, H.F. Xiao, Z.L. Liu, T. Zhao, H. Jia, J.H. Yang, B.J. Eggleton, Y.H. Tian, Reconfigurableon-chip mode exchange for mode-division multiplexing optical networks. J. Lightwave Technol. **37**(3), 1008–1013 (2019)
19. Y. Fazea, V. Mezhuyev, Selective mode excitation techniques for mode-division multiplexing: a critical review. Opt. Fiber Technol. **45**, 280–288 (2018)
20. T. Umezawa, T. Sakamoto, A. Kanno, N. Yamamoto, T. Kawanishi, High speed 2-D photodetector array for space and mode-division multiplexing fiber communications. J. Lightwave Technol. **36**(17), 3684–3692 (2018)
21. J.X. Li, C.K. Cai, J.B. Du, S.L. Jiang, L. Ma, L.L. Wang, L. Zhu, A.D. Wang, M.J. Li, H. Chen, Ultra-low-noise mode-division multiplexed WDM transmission over 100-km FMF based on a second-order few-mode Raman amplifier. J. Lightwave Technol. **36**(16), 3254–3260 (2018)
22. L.G. Wright, D.N. Christodoulides, F.W. Wise, Controllable spatiotemporal nonlinear effects in multimode fibres. Nat. Photonics **9**(5), 306–310 (2015)
23. L.G. Wright, Z.M. Ziegler, P.M.Z.M. Lushnikov, Z. Zhu, M.A. Eftekhar, Multimode nonlinear fiberoptics: massively parallel numerical solver, tutorial, and outlook. IEEE J. Sel. Top. Quant. **24**(3), 5100516 (2018)
24. U. Tegin, B. Ortac, Spatialtemporal instability of femtosecond pulses in graded-index multimode fibers. IEEE Photonics Technol. Lett. **29**(24), 2195–2198 (2017)
25. P. Balla, S. Buchand, G.P. Agrawal, Effect of Raman scattering on soliton interactions in optical fibers. J. Opt. Soc. Am. B **34**(6), 1247–1254 (2017)
26. M. Conforti, C.M. Arabi, A. Mussot, A. Kudlinski, Fast and accurate modeling of nonlinear pulse propagation in graded-index multimode fibers. Opt. Lett. **42**(19), 4004–4007 (2017)
27. S. Buch, G.P. Agrawal, Intermodal soliton interaction in nearly degenerate modes of a multimode fiber. J. Opt. Soc. Am. B **33**(11), 2217–2224 (2016)
28. S. Perret, G. Fanjoux, L. Bigot, G. Millot, J.M. Dudley, T. Sylvestre, Supercontinuum generation by intermodal four-wave mixing in a step-index few-mode fibre. Apl. Photonics **49**(2), 022905 (2018)
29. R. Dupiol, A. Bendahmane, K. Krupa, J. Fatome, A. Tonello, M. Fabert, V. Couderc, S. Wabnitz, G. Millot, Intermodal modulational instability in graded-index multimode optical fibers. Opt. Lett. **42**(17), 3419–3422 (2017)
30. M. Guasoni, Generalized modulational instability in multimode fibers: wideband multimode parametric amplification. Phys. Rev. A **92**(3), 033849 (2015)
31. B. Abdelkrim, K. Katarzyna, T. Alessandro, Seeded intermodal four-wave mixing in a highly multimode fiber. J. Opt. Soc. Am. B **35**(2), 295–301 (2018)
32. J.H. Li, K.S. Chiang, K.W. Chow, Modulation instabilities in two-core optical fibers. J. Opt. Soc. Am. B **28**(7), 1693–1701 (2011)
33. J.H. Li, K.S. Chiang, B.A. Malomed, K.W. Chow, Modulation instabilities in birefringent two-core optical fibres. J. Phys. B: Atomic, Molecul. Optic. Phys. **45**(16), 165404 (2012)
34. J.H. Li, H. Zhou, K.S. Chiang, S.R. Xiao, Modulation instabilities in equilateral three-core optical fibers. J. Opt. Soc. Am. B **33**(11), 2357–2367 (2016)
35. J.H. Li, K.S. Chiang, C.R. Li, Modulation instability in collinear three-core optical fibers. J. Opt. Soc. Am. B **34**(12), 2467–2477 (2017)
36. A. Alim, M. Youssoufa, A. Mohamadou, Effects of higher-order nonlinear dispersions on modulational instability in a three-core coupler with negative index material channel and saturable nonlinearity. Optik **149**, 5–21 (2017)
37. A.K.S. Ali, K. Nithyanandan, K. Porsezian, Theoretical investigation of modulation instability in a threecore coupler with negative index material channel. Phys. Lett. A **379**(3), 223–229 (2015)
38. A.K.S. Ali, K. Nithyanandan, K. Porsezian, A.I. Maimistov, Modulation instability in a triangular three-core coupler with a negative-index material channel. J. Opt. **18**(3), 035102 (2016)
39. Y.J. Xiang, S.C. Wen, X.Y. Dai, D.Y. Fan, Modulation instability in nonlinear oppositely directed coupler with a negative-index metamaterial channel. Phys. Rev. E **82**(5), 056605 (2010)
40. P.H. Tatsing, A. Mohamadou, C. Bouri, C.G.L. Tiofack, T.C. Kofane, Modulation instability in nonlinear positive-negative index couplers with saturable nonlinearity. J. Opt. Soc. Am. B **29**(12), 3218–3225 (2012)
41. K. Nithyanandan, R.V.J. Raja, K. Porsezian, Modulational instability in a twin-core fiber with the effect of saturable nonlinear response and coupling coefficient dispersion. Phys. Rev. A **87**(4), 043805 (2013)

42. A. Mohamadou, P.H. Tatsing, C.G.L. Tiofack, C.B. Tabi, T.C. Kofane, Effects of higher order nonlinearities on modulational instability in nonlinear oppositely directed coupler. J. Mod. Opt. **61**(20), 1670–1678 (2014)
43. D. Djidna, G. Betchewe, A. Alim, A. Mohamadou, Cross-phase modulation instability in an elliptical birefringent positive-negative index coupler with self-steepening and intrapulse Raman Scattering effects. Optik **185**, 726–739 (2019)
44. E.O. Alves, W.B. Cardoso, A.T. Avelar, Modulation instability in a nonlinear oppositely directed coupler with saturable nonlinearities and high-order effects. J. Opt. Soc. Am. B **33**(6), 1134–1142 (2016)
45. A.K. Shafeeque Ali, K. Porsezian, T. Uthayakumar, Influence of self-steepening and intrapulse Raman scattering on modulation instability in oppositely directed coupler. Phys. Rev. E **90**(4), 042910 (2014)
46. J.G. Zhang, X.Y. Dai, L.F. Zhang, Y.J. Xiang, Y.F. Li, Modulation instability in the oppositely directed coupler with a quadratic nonlinearity. J. Opt. Soc. Am. B **32**(1), 1–8 (2015)
47. K. Porsezian, A.K.S. Ali, K. Nithyanandan, A theoretical study on threshold conditions of modulation instability in oppositely directly couplers. J. Opt. **18**(12), 125502 (2016)
48. G.P. Agrawal, *Applications of Nonlinear Fiber Optics* (Academic Press, Burlington, 2008)
49. P. Mohanraj, R. Sivakumar, Role of higher order nonlinearities in the instability spectra of two core oppositely directed saturated coupler. Optik **192**, 162904 (2019)
50. P. Mohanraj, R. Sivakumar, A. Joseph, Impact of higher order dispersions and nonlinearities on instability criterion of oppositely directed coupler in the presence of negative index material channel. Optik **255**, 168705 (2022)
51. P. Mohanraj, R. Sivakumar, Saturable higher nonlinearity effects on the modulational instabilities in three-core triangular configuration couplers. J. Opt. **23**, 045502 (2021)
52. P. Mohanraj, R. Sivakumar, A.M. Arulanandham, K.V. Gunavathy, Study on modulational instability in three-core nonlinear directional saturated coupler with septic nonlinearity. Optic. Quantum Electron. **54**(6), 386 (2022)
53. P. Mohanraj, R. Sivakumar, A.M. Arulanandham, S. Vinoth, Impact of saturation on cross-phase instability in birefringent oppositely directed coupler with higher-order nonlinearities. Indian J. Phys. **96**(12), 3613–3626 (2022)
54. P. Mohanraj, R. Sivakumar, A.M. Arulanantham, M. Vijayakumar, The role of septic saturation on the cross-phase instability in two-core birefringent oppositely directed PIM-NIM coupler. Phys. Lett. A. **450**, 128366 (2022)
55. I.R. Litchinitser, N.M. Gabitov, A.I. Maimistov, Optical bistability in a nonlinear optical coupler with a negative index channel. Phys. Rev. Lett. **99**, 113902 (2007)
56. Z. Xian-Qiong, X. An-Ping, Generation of time-dependent ultra-short optical pulse trains in the presence of self-steepening effect. Chinese Phys. B. **18**(2), 624 (2009)
57. X. Yuanjiang, W. Shuangchun, D. Xiaoyu, F. Diayuan, Modulation instability in nonlinear oppositely directed coupler with a negative-index meta material channel. Phy. Rev. E **82**, 056605 (2010)